iScience

CellPress
OPEN ACCESS

Article

Spatiotemporal Gradient and Instability of Wnt Induce Heterogeneous Growth and Differentiation of Human Intestinal Organoids

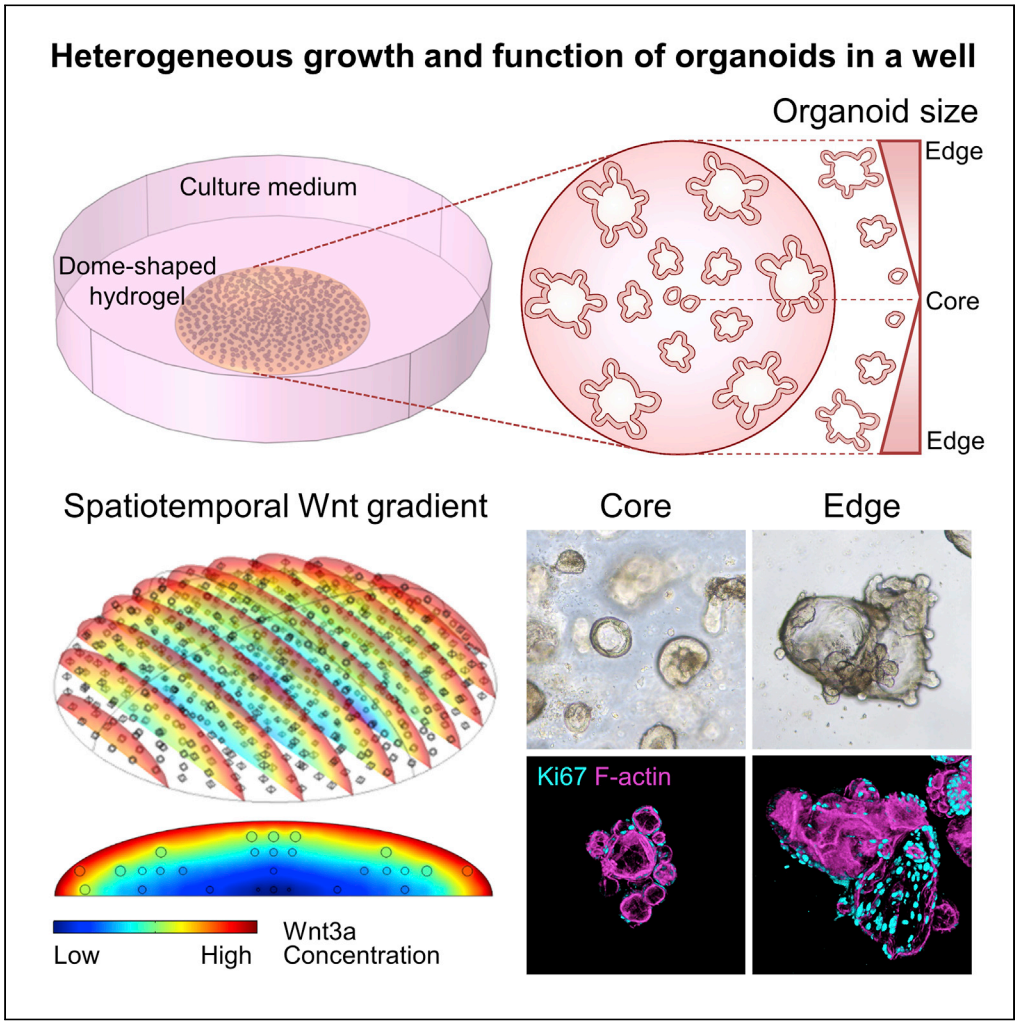

Woojung Shin, Alexander Wu, Soyoun Min, Yong Cheol Shin, R. Y. Declan Fleming, S. Gail Eckhardt, Hyun Jung Kim

hyunjung.kim@utexas.edu

HIGHLIGHTS

Normal intestinal organoids show heterogeneous growth and function inside the ECM

Instability of Wnt3a and its diffusion limitation induce spatiotemporal Wnt3a gradient

Conventional organoid culture may cause false interpretation due to the heterogeneity

Shin et al., iScience *21*, 101372
August 21, 2020
https://doi.org/10.1016/j.isci.2020.101372

iScience

CellPress
OPEN ACCESS

Article

Spatiotemporal Gradient and Instability of Wnt Induce Heterogeneous Growth and Differentiation of Human Intestinal Organoids

Woojung Shin,[1] Alexander Wu,[1] Soyoun Min,[1] Yong Cheol Shin,[1] R. Y. Declan Fleming,[2,3] S. Gail Eckhardt,[2] and Hyun Jung Kim[1,2,4,5,*]

SUMMARY

In a conventional culture of three-dimensional human intestinal organoids, extracellular matrix hydrogel has been used to provide a physical space for the growth and morphogenesis of organoids in the presence of exogenous morphogens such as Wnt3a. We found that organoids embedded in a dome-shaped hydrogel show significant size heterogeneity in different locations inside the hydrogel. Computational simulations revealed that the instability and diffusion limitation of Wnt3a constitutively generate a concentration gradient inside the hydrogel. The location-dependent heterogeneity of organoids in a hydrogel dome substantially perturbed the transcriptome profile associated with epithelial functions, cytodifferentiation including mucin 2 expression, and morphological characteristics. This heterogeneous phenotype was significantly mitigated when the Wnt3a was frequently replenished in the culture medium. Our finding suggests that the morphological, transcriptional, translational, and functional heterogeneity in conventional organoid cultures may lead to a false interpretation of the experimental results in organoid-based studies.

INTRODUCTION

The development of three-dimensional (3D) organoid culture has revolutionized the *in vitro* cultures of human primary epithelial cells because it allows the stable and robust cultures of primary cells with the maintenance of stem and differentiated cells (Clevers, 2016; Sato et al., 2011; Yui et al., 2012). Human intestinal organoids have provided a rapid regeneration of primary intestinal epithelium (Sato et al., 2011) pertinent to various gastrointestinal diseases (Clevers, 2016; Dedhia et al., 2016; Schwank et al., 2013). Exogenous morphogens such as Wnt3a, R-Spondin, and Noggin are constitutively required for the conventional intestinal organoid cultures (Sato et al., 2011; Sugimoto and Sato, 2017). Among the three major morphogens, Wnt3a is considered as the essential protein in the intestinal organoid culture because the proliferation of stem cells is primarily governed by the Wnt signaling pathway (Koch, 2017; Mah et al., 2016; Sato and Clevers, 2013).

Human intestinal organoids have been cultured in an extracellular matrix (ECM) hydrogel such as Matrigel (Drost et al., 2016; Ohta and Sato, 2014), where the solidified 3D hydrogel that forms a dome shape in a well plate provides a space to grow organoid fragments into a self-organized 3D cyst or a budding microstructure with crypt-villus domains in ~7 days (Sato et al., 2011; Sugimoto and Sato, 2017). This method is relatively convenient, easy to handle, and feasible to a multi-well plate (e.g., 24-, 48-, and 96-well plates) to provide a 3D scaffold matrix for holding organoids to grow into 3D structure. The protocol of organoid culture has been optimized and widely implemented by various research groups (Ettayebi et al., 2016; Li et al., 2014). However, due to the complex culture condition (Holloway et al., 2019), inter-heterogeneity of the biopsy-derived organoids has often been observed between organoid lines (Michels et al., 2019; Urbischek et al., 2019) or the quality of conditioned medium for supplying the major morphogens (Fatehullah et al., 2016). Various efforts have been made to overcome these challenges by increasing the number of experimental replicates, testing multiple lines, and validating the effect of different passage numbers to improve experimental statistics. Interestingly, organoids grown in a dome-shaped Matrigel scaffold have shown heterogeneity in size and shape, which has been reportedly observed in previous studies (Kassis et al.,

[1]Department of Biomedical Engineering, The University of Texas at Austin, 107 W. Dean Keeton St., Austin, TX 78712, USA

[2]Department of Oncology, Dell Medical School, The University of Texas at Austin, Austin, TX 78712, USA

[3]Department of Surgery and Perioperative Care, Dell Medical School, The University of Texas at Austin, Austin, TX 78712, USA

[4]Department of Medical Engineering, Yonsei University College of Medicine, Seoul 03722, Republic of Korea

[5]Lead Contact

*Correspondence: hyunjung.kim@utexas.edu

https://doi.org/10.1016/j.isci.2020.101372

2019; Nanki et al., 2020). Yet, the underlying mechanism of this intra-heterogeneity in a Matrigel dome is unclear.

We hypothesized that a gradient of morphogens that orchestrates the proliferation of organoids in a Matrigel dome may be a critical factor that causes the heterogeneity of organoids inside the dome. Wnt3a is one of the most critical morphogens in organoid cultures; however, Wnt3a is notably unstable in a serum-free medium because of its hydrophobic characteristics (Mihara et al., 2016; Tuysuz et al., 2017). The diffusion limitation of Wnt3a into the Matrigel core may also be a causative factor of the spatiotemporal morphogen gradient of Wnt3a inside the Matrigel dome that contains organoids. More importantly, it is supposed that this location-dependent distribution of heterogeneous organoids in the Matrigel may show significant perturbations in transcriptome profiles and epithelial functions. As cultured organoids have been widely used for investigating the efficacy and toxicity of pharmaceuticals (Crespo et al., 2017; Mochel et al., 2017), morphogenesis and developmental process (Fair et al., 2018; Fatehullah et al., 2016), and patient specificity of therapeutics (Aberle et al., 2018; Mochel et al., 2017), it is important to understand if the phenotypic intra-heterogeneity induces the spatial perturbation of organoid functions as well as the compromised reproducibility.

In this study, we investigated the effect of morphogen gradient on a conventional organoid culture that produces the consequent intra-heterogeneity of organoids in growth, morphology, cytodifferentiation, and epithelial cell function. To prove our hypothesis, we applied high-resolution imaging, computational simulation, and transcriptomic profiling to quantify the intra-heterogeneity of organoids in response to the Wnt3a perturbation. By manipulating the quantitative profile of Wnt3a at various culture milieus, we discovered how the spatiotemporal gradient and the instability of Wnt3a induce heterogeneous growth, differentiation, and functions of human intestinal organoids. Finally, we discussed an ensuing impact of our discovery on the interpretation of experimental results when using the conventional cultures of intestinal organoids.

RESULTS

Morphological Heterogeneity of Intestinal Organoids in a Matrigel Dome

This study was inspired by a careful observation of the heterogeneous morphology of non-diseased, normal human intestinal organoids embedded in a Matrigel dome in a 24-well plate. We consistently observed, using the stitched phase contrast micrographs, that the size of organoids in the core (Figure 1A, "Core") was substantially smaller than the ones in the edge (Figure 1A, "Edge") when the entire area of a well was scanned. To quantitatively assess the size heterogeneity, the dome area was divided into three "bull's eye" regions (core, intermediate, and edge) and indicated with different colors (Figure 1A, left). High-power magnification images revealed that the organoids at the core (light blue) or the intermediate location (pale blue) show significantly smaller size than the organoids at the edge (Figure 1B; dark blue). When we performed the same morphological analysis of tumor organoids derived from colorectal cancer (CRC) tissue, we neither observed any size heterogeneity at different locations (Figure 1C) nor found a significant difference in the size of CRC organoids regardless of the location inside the Matrigel dome (Figure 1D). Thus, we confirmed that the normal intestinal organoids derived from multiple donors considerably undergo heterogeneous growth in conventional organoid culture, whereas the tumor-derived organoids did not.

Heterogeneity in Organoid Growth Governed by the Spatiotemporal Gradient of Wnt3a

We hypothesized that the morphological difference between normal and CRC organoids originates from the morphogen concentration, especially Wnt3a, in the culture medium because the growth of normal intestinal organoids is predominantly controlled by the Wnt signaling pathway, whereas it has been shown that CRC organoids do not necessarily require exogenous Wnt morphogen (Sato et al., 2011). Thus, we first profiled the concentration of Wnt3a in the proliferation medium over 48 h, a typical time frame that the proliferation medium is incubated in a well plate, by a cell-based luciferase assay (Figure 2A). The concentration of Wnt3a decreased exponentially when the medium was incubated at both 4°C and 37°C, regardless of the material of the container wherein the proliferation medium was incubated (Figure S1). When organoids were suspended in the proliferation medium without Matrigel, Wnt3a concentration dropped the most (Figure 2B, "+Organoids," maximum Wnt3a reduction rate, ~50.1 ng/mL·h) compared with the control (Figure 2B, "Control," maximum Wnt3a reduction rate, ~35.6 ng/mL·h) suggesting that the organoid itself contributes to reducing the level of Wnt3a possibly by the cellular uptake. A group with Matrigel alone

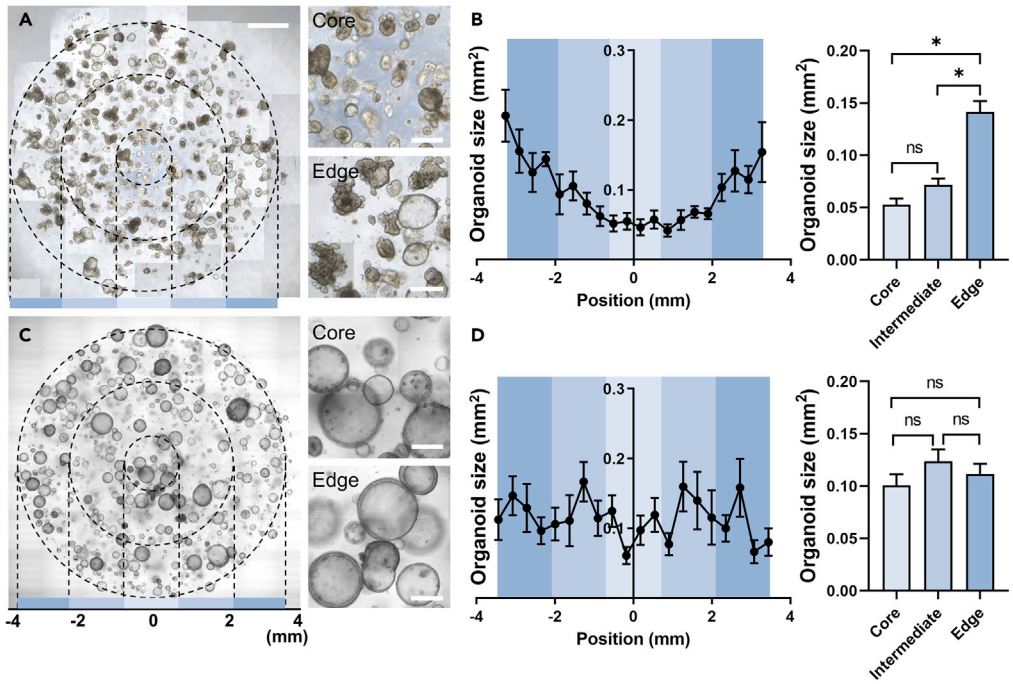

Figure 1. Morphological Heterogeneity Is Robust in Normal Organoid Cultures

(A) A stitched micrograph of a Matrigel dome that embeds normal colonic organoids cultured for 6 days (left). A bull's eye (dotted circles) divided into three regions was used for the quantification. The core, intermediate, and edge regions are indicated with light, pale, and dark blue colors, respectively. High-magnification images focusing on the core (right top) and edge (right bottom) display significant differences in organoid size.

(B) The size distribution of normal human intestinal organoids across the entire matrix dome area corresponding to the stitched image in "A" (left) and the mean organoid size in each region (right). A total of four Matrigel domes that contain normal intestinal organoids were analyzed to estimate the cross-sectional area of individual organoids using ImageJ. The color in each column is matched to the corresponding location in (A).

(C) A stitched image of a Matrigel dome that contains CRC organoids cultured for 6 days under the same culture condition provided in (A) (left). High-power magnified images confirm that the CRC organoids in the core (right top) are morphologically similar to those in the edge (right bottom).

(D) The size distribution of CRC organoids across the dome area corresponding to the stitched image in (C) (left), and the mean organoid size in each region (right). Similar to the normal organoid, four Matrigel domes that contain CRC organoids were analyzed to obtain the cross-sectional area of individual CRC organoids.

A color bar at the bottom in both (A) and (C) shows the matched region in (B) and (D). Scale bars, 1 mm in the left images in both (A) and (C) and 200 μm in the right insets in both (A) and (C). Data are represented as mean ± SEM. One-way ANOVA with multiple comparison was performed to evaluate statistical significance of the differences. *$p < 0.05$; ns, not significant.

(Figure 2B, "+Matrigel") showed a more rapid decrease compared with the control (maximum Wnt3a reduction rate at ~45.1 ng/mL·h), implicating that Wnt3a may be attracted by Matrigel. When organoids were embedded in Matrigel (Figure 2B, "+Matrigel + Organoid"), the profile of Wnt3a concentration was similar to that of "+Matrigel" over time. Taken together, two additional factors were identified that can alter the concentration of Wnt3a: the cellular uptake of Wnt3a by organoids and the diffusion limitation for Wnt3a into the Matrigel.

Based on the exponential decrease of Wnt3a concentration in the medium (Figures 2A and 2B) as well as the heterogeneous size difference of organoids at different locations (Figures 1A and 1B), we postulated that organoids embedded in the core of a dome might grow under insufficient, or even a lack of, Wnt3a compared with the organoids at the edge. To examine the effect of the location where the organoids grow during proliferation, we harvested organoids in the core (3 mm in diameter from the center) and edge (rest of the area except the core), independently, using a cut pipette tip (Figures 2C and S2). To collect the core organoids but excluding the edge organoids on the top surface of a dome, a cell scraper

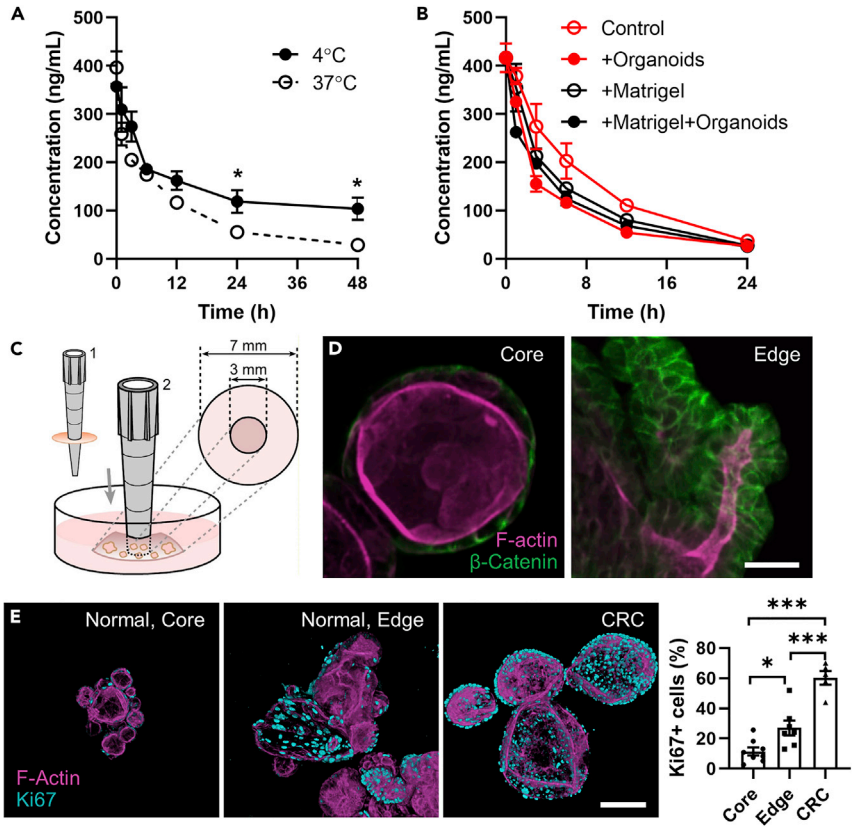

Figure 2. Spatiotemporal Gradient and Instability of Wnt3a Induce Heterogeneous Proliferation in Normal Intestinal Organoids

(A) The temporal stability of Wnt3a in a complete medium incubated at either 4°C or 37°C (N = 3).

(B) The concentration profile of Wnt3a incubated in the medium alone (Control), the medium containing organoids (+Organoids), Matrigel (+Matrigel), or both (+Matrigel + Organoids) at 37°C for 24 h. In each condition, supernatant (500 μL) in each well of a 24-well plate was collected at each time point for the quantification (N = 3). The difference between the "Control" and "+Organoids" is statistically significant at 12 h ($p < 0.05$).

(C) A schematic depicting the method to collect core and edge organoids, separately. A 200-μL tip was first cut to generate an outer diameter of 3 mm using a sterile scalpel, and core Matrigel was harvested using a P200 micropipette. The remaining edge organoids were harvested separately afterward.

(D) Visualization of the expression of phosphorylated β-catenin (green) in the organoids harvested from either the core or edge of the organoid cultured for 3 days. The F-actin (magenta) was counterstained to confirm the structure of an organoid. Scale bar: 25 μm.

(E) Expression profile of the proliferative cells (Ki67, cyan) in normal (core and edge) or CRC organoids and its quantification (right; N = 8). Scale bar, 100 μm. Data are represented as mean ± SEM. Two-way ANOVA was performed in (A), and one-way ANOVA was performed in (E) to evaluate statistical significance of the differences. *$p < 0.05$, ***$p < 0.0001$.

(5 mm width) was used to cut out the top part of the Matrigel dome before the core harvest (Figures S2A and S2B; Steps 1–3). Once we harvested the net core and the edge organoids, we first stained the core and edge organoids with phosphorylated β-catenin, respectively, to examine whether the canonical Wnt signaling is active on each organoid group. It is noted that organoids harvested from the core showed a localized signal of β-catenin on the cell membrane. However, the fluorescence signal of phosphorylated β-catenin was more broadly expressed in the cytoplasm of the organoids harvested from the edge, suggesting that the canonical Wnt signaling is more active in the edge organoids than the core organoids (Figure 2D). When the expression of Ki67, a proliferative marker, was visualized in the core versus edge organoids, a minimal number of Ki67-positive cells was observed in the core organoid (11.45 ± 2.65%; Figure 2E, "Normal, Core"), whereas the level in the edge organoids was significantly higher (26.97 ± 4.91%, $p < 0.05$; Figure 2E, "Normal, Edge"). On the contrary, CRC organoids showed robust expression of Ki67 regardless

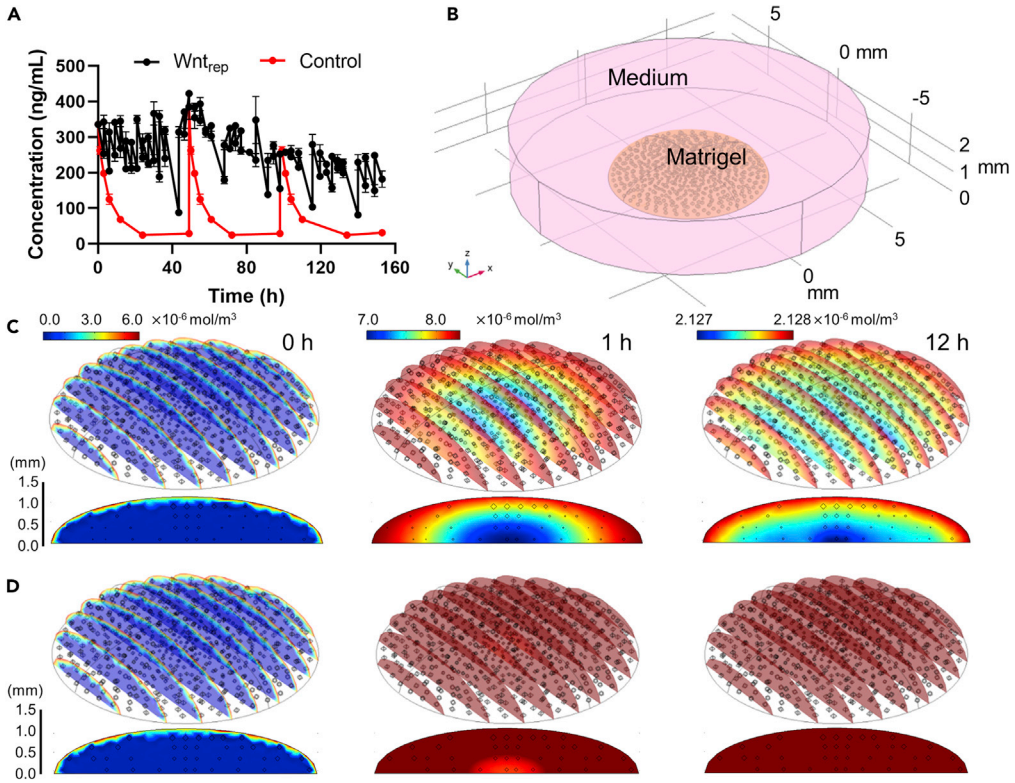

Figure 3. Repeated Replenishment of Wnt3a Reduces the Gradient of Wnt3a in a Matrigel Dome

(A) The concentration profile of Wnt3a when the organoid culture medium was replenished every 3 h (Wnt$_{rep}$) versus every other day (Control) for ~6.5 days. Data are represented as mean ± SEM.

(B–D) (B) A graphical geometry of the microenvironment of a conventional organoid culture applied for the computational simulation. The diameter and height of Matrigel dome were set to 7 and 1.2 mm, respectively, based on the actual measurements. The heatmap profiles of the Wnt3a concentration inside the hydrogel dome during the conventional culture (C) versus Wnt-replenished condition (D). Concentration profiles at 0, 1, and 12 h are presented with the angled (upper) and vertical cross-cut views (lower) in each condition. Modular color scales show the concentration range used at each time point.

of the position in the Matrigel dome (60.22 ± 4.55%, Figure 2E, "CRC"), explaining the reason why CRC organoids grow evenly throughout the entire Matrigel (Figures 1C and 1D).

Effect of Wnt Replenishment on the Intra-heterogeneity of Organoids

To confirm if the rapid decrease of Wnt3a concentration is a major driver of the intra-heterogeneity of organoid growth and proliferation, we manually replenished Wnt3a by changing the proliferation medium every 3 h (Wnt$_{rep}$; Figure 3A) followed by computational and morphological analyses. First, we simulated the spatiotemporal gradient of Wnt3a created in a Matrigel dome under the Wnt-replenished condition (Wnt$_{rep}$) compared with the conventional culture condition without Wnt replenishment (Control) using a 3D computational modeling (Figure 3). In the simulation setup, the transport of diluted species was computed to calculate the Wnt3a concentration, and Fick's second law with reaction terms was applied to reflect diffusion and concentration decrease of Wnt3a. A 3D geometry of a Matrigel dome was built based on the actual shape, where the volume of a Matrigel dome and proliferation medium used in the culture were set as 30 and 500 μL, respectively, in the simulation (Figure 3B). Boundary conditions and constants were set based on the experimental results obtained from Figures 2 and 3 as well as other studies (Table S1 and Figure S3, see Transparent Methods). In the conventional culture condition, the concentration gradient of Wnt3a was instantly generated within 1 h, where the gradient was robustly maintained up to 12 h between the core and the edge (Figure 3C). On the contrary, the Wnt replenishment considerably resolved the gradient generation of Wnt3a inside the dome, resulting in the uniform distribution of the Wnt3a molecules regardless of the location as a function of time (Figures 3D and S4).

It was noted that three major factors could possibly contribute to the generation of the Wnt3a gradient; uptake of Wnt3a by organoid cells, diffusion limitation of Wnt3a in the Matrigel dome, and Wnt3a instability. To identify the critical trigger of the generation of the Wnt3a gradient, we performed the computational simulation by excluding the effect of each component one at a time. When we excluded the effect of cellular uptake of Wnt3a (Figure S5A), the gradient of Wnt3a in the dome showed no significant difference compared with the conventional culture (Figure 3), suggesting that the effect of Wnt uptake by the organoid cells on the consistent gradient of Wnt3a is minimal. However, when we simulated the non-diffusion limitation regime inside the Matrigel (i.e., the diffusion coefficient of Wnt3a in Matrigel was identical to that in the culture medium), the Wnt3a concentration profile was uniform across the gel regardless of the location (Figure S5B), suggesting that the diffusion limitation inside the Matrigel remarkably contributes to creating the Wnt3a gradient. When we neglected the exponential decline of Wnt3a concentration in the simulation, we lost the Wnt3a gradient (Figure S5C), suggesting that the Wnt instability is also a critical factor that induces Wnt gradient inside the hydrogel dome. Although the cellular uptake was observed to be minimal, we found that there is subtle local gradient around the organoids within the formed gradient at 12 h in the control group (Figure S6).

To verify the effect of Wnt3a gradient caused by the diffusion limitation and the Wnt instability on both proliferation and differentiation of organoids, we next examined how the enhanced Wnt3a supply can modulate the intra-heterogeneity of Wnt3a and improve the phenotype of organoids. To avoid the depletion of Wnt3a by the diffusion limitation and Wnt instability, we intentionally added Wnt3a every 3 h (Wnt_{rep}), where the organoids in the Wnt_{rep} group grew significantly ($p < 0.0001$) bigger (Figure S7B) than the control (Figure S7A; no replenishments) across the entire area of the dome. Both the core and edge organoids were ~7.9- and ~9.5-fold bigger, respectively, in each sector on day 6; nonetheless, the parabolic distribution pattern of the organoid size was similar to the control (Figure 4A). We also found that the "aged organoids" that contain shed out cells accumulated in the luminal domain of an organoid were much dominant in the conventional cultures, whereas the organoids in the Wnt_{rep} condition showed significantly ($p < 0.05$) lower numbers of shed cells in the organoid lumen assessed by phase contrast microscopy, suggesting that the population of "dying cells" in individual organoids in the conventional culture is significantly higher than the organoids in the Wnt-replenished condition (Figure 4B).

Impact of Intra-heterogeneity on Epithelial Differentiation and Function

Next, we investigated whether the spatiotemporal Wnt gradient followed by the structural heterogeneity of organoids in the Matrigel dome also perturbs the transcriptome profiles and eventually, alters the epithelial differentiation and function of organoids. After we cultured organoids in either Wnt-replenished or conventional culture conditions for 3 days once passaged, we switched to the differentiation medium in both experimental groups for additional 3 days to investigate how the intra-heterogeneity perturbs the gene expressions pertinent to the fundamental epithelial functions. First, we performed a qPCR analysis that covers 59 genes germane to the intestinal epithelial functions to assess the transcriptomic profile of intestinal organoid epithelium collected from core versus edge in each culture condition. The hierarchical heatmap revealed that the organoids grown in the Wnt_{rep} condition globally upregulated the gene expressions compared with the non-replenished control in both core and edge locations (Figure 4C). The volcano plots visualized the quantitative fold increase of the genes expressed in the organoids grown in the Wnt-replenished condition compared with the control, where 14 genes were significantly ($p < 0.05$) upregulated in the core region, whereas only 2 genes were identified in the edge region (Figure 4D). We found that the core organoids conditioned in the Wnt-replenished medium showed higher expression of the genes associated with epithelial barrier function (*CDH1, VAV2, KLF4*, and *OCLN*), structural shape (*SNAI1* and *GSN*), and cell growth and differentiation (*ERBB2, SOX9, CALB2, GFM1, DLL4, NOTCH1, HNF1A*, and *EEF1B2*) (Figures 4D and 4E, "Core"). On the contrary, only two genes, *EPRS,* which encodes glutamyl-prolyl-tRNA synthetase protein, and *SHROOM3,* which regulates cell shape, were upregulated in the edge organoids (Figures 4D and 4E, "Edge"), suggesting that a minimal change in epithelial function is anticipated by the continuous and sufficient exposure to Wnt proteins.

We also confirmed the intra-heterogeneity at the protein level, where a representative goblet cell marker, mucin 2 (MUC2), that contributes to the mucus production was visualized on both the core and edge organoids pre-conditioned with the Wnt-replenished or control medium for 3 days followed by the differentiation medium for additional 3 days (Figure 4F). Immunofluorescence imaging revealed that the Wnt-replenished condition contributed to significantly enhance the averaged MUC2 expression per

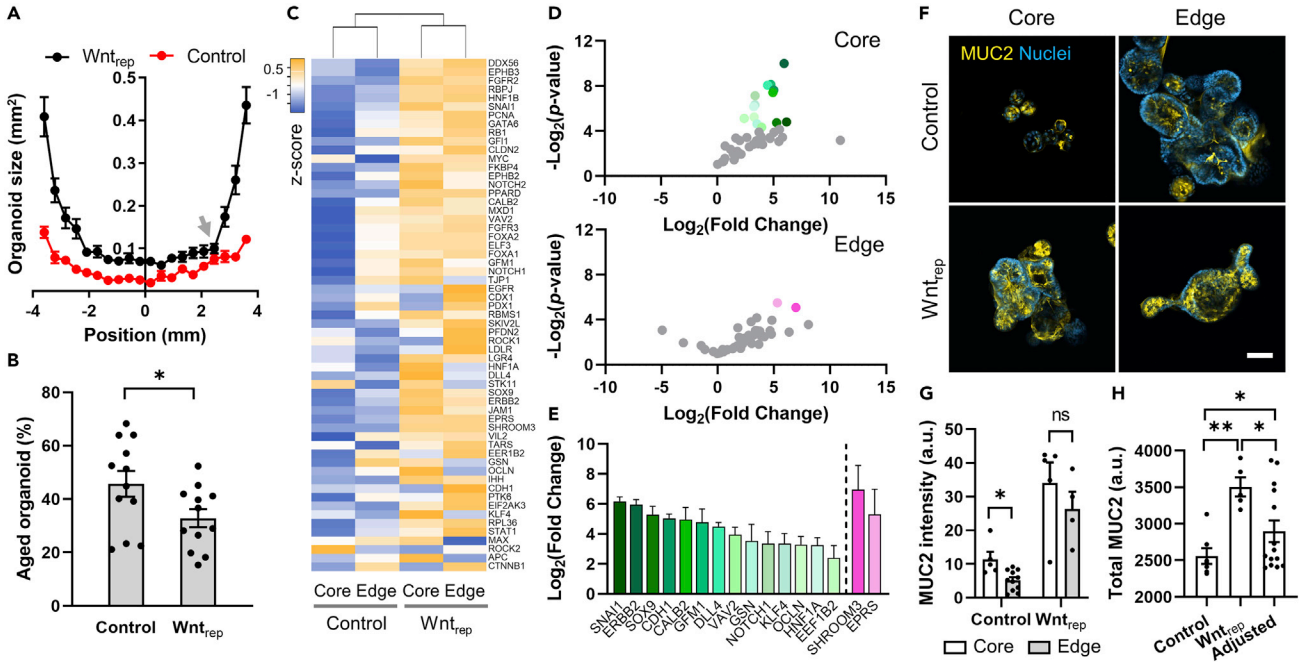

Figure 4. Reduced Intra-heterogeneity of the Wnt Gradient Contributes to Enhancing the Organoid Growth and Epithelial Function of the Core Organoids

(A) The size distribution pattern of the organoids cultured in the conventional (Control) or Wnt-replenished condition (Wnt$_{rep}$) for 6 days. The cross-sectional area of 20 organoids along different lines crossing the center (position at 0 mm) of the Matrigel circle provided in Figure S7 was quantified using ImageJ. All the data points provided show statistical significance ($p < 0.05$) except the point indicated by a gray arrow (N = 23).

(B) The abundance of aged organoids at day 6 in cultures in the conventional (Control) or Wnt-replenished cultures (Wnt$_{rep}$) quantified by the assessment of phase contrast image. N = 12.

(C) A hierarchical heatmap profiling the expression of 59 genes related to physiological epithelial functions of the organoids cultured in either conventional (Control) or Wnt-replenished condition (Wnt$_{rep}$) followed by the locational collection of the core versus edge (N = 3).

(D) The volcano plots displaying the significantly ($p < 0.05$) upregulated genes (colors coded with green and pink, whereas non-significant genes were colored with gray) when the organoids were cultured in the Wnt-replenished condition compared with the conventional cultures. Once cultured in each condition, organoids were collected from the core (top) and edge (bottom), respectively, and then used for the qPCR assessment.

(E) The detailed expression profile of the genes identified in (D) with statistical significance (N = 3). The green and pink columns indicate the significantly upregulated genes in the core and edge organoids, respectively.

(F) Visualization of MUC2 expressions in the organoids cultured in either conventional (Control) or Wnt-replenished condition (Wnt$_{rep}$) for 3 days followed by the incubation with the differentiation medium for additional 3 days. Scale bar, 100 μm.

(G) Quantification of the averaged MUC2 expression per organoids presented in "F" via image analysis (Control-core, N = 5, Control-edge, N = 11, Wnt$_{rep}$-core, N = 5, Wnt$_{rep}$-edge, N = 4).

(H) Quantitative estimation of the total MUC2 expression of the organoids in a well, cultured in different conditions (Control versus Wnt$_{rep}$) by multiplying the integrative MUC2 expression per organoid and the actual number or organoids in each region (core versus edge). The "Adjusted" MUC2 intensity was a theoretical estimation of the total MUC2 expression when the core organoids cultured in a conventional condition were assumed not undergoing the heterogeneous Wnt3a gradient inside the Matrigel dome. The numbers of organoids applied for the calculation, 75 (core) and 297 (edge) in both "Adjusted" and "Control"; 75 (core) and 220 (edge) in "Wnt$_{rep}$." Three stitched images were used for quantification. Control, N = 7, Wnt$_{rep}$, N = 5, Adjusted, N = 14. Data are represented as mean ± SEM. One-tailed and two-tailed unpaired t tests were performed in (A) and (B), respectively, and two-way and one-way ANOVA was performed in (G) and (H), respectively, to evaluate statistical significance of the differences. *$p < 0.05$, **$p < 0.001$.

organoid in both the core and edge organoids ($p < 0.05$) than the conventional culture protocol (Figure 4G). However, the Wnt-replenished condition did not show notable heterogeneity in MUC2 expression (Figure 4G). Based on the quantitative analysis of immunofluorescence images, we computed the total expression of MUC2 in a well by considering the total number of core and edge organoids (Figure 4H). We found that the total MUC2 expression in the control was significantly lower than that in both Wnt-replenished (~73.0%, $p < 0.001$) and "Adjusted" conditions (~88.2%, $p < 0.05$) that theoretically normalized the size of the core organoids to the ones in the edge (i.e., the uniform size distribution of organoids similar to the case of CRC organoids) (Figure 4H). This result strongly suggests that the expression of physiologically important MUC2 protein was decreased in the core organoids under the conventional culture

condition, which considerably compromises the overall outcome and result interpretation. When the Wnt-replenished or control medium was kept for 6 days, the averaged MUC2 expression per organoid was higher in the control group, both in core and edge (Figure S8).

In summary, we discovered that the diffusion limitation and Wnt instability play a pivotal role in creating the Wnt3a gradient in the Matrigel dome in conventional organoid culture. As a consequence, individual organoids in a dome undergo heterogeneous patterns in morphology, proliferation, differentiation, and gene expression, which may cause a compromised reproducibility or a false interpretation of the experimental results.

DISCUSSION

In this study, we examined how the spatiotemporal Wnt gradient stemmed from the Wnt instability and diffusion limitation within the hydrogel is generated in the conventional culture of intestinal organoids. We discovered that the concentration gradient of Wnt3a in a Matrigel dome results in the spatial intra-heterogeneity in both growth and epithelial function of organoids. Our study revealed that organoids embedded in the Matrigel core undergo a deficiency of Wnt signal compared with the edge; thereby the growth was significantly impaired. The computational simulation, as well as the immunofluorescence imaging targeting the canonical Wnt signaling pathway, confirmed that the pseudo-maintenance of the Wnt3a level in the culture medium could remarkably minimize the gradient of Wnt3a concentration, which in part reduced the heterogeneity of epithelial function.

Intestinal organoids are used in diverse research fields, including developmental biology, gastroenterology, pharmacology, toxicology, and tissue engineering (Clevers, 2016; Fatehullah et al., 2016; Nakamura and Sato, 2018). Because organoids are derived from human donors, organoids can retain traits of a donor, including genetic variants associated with the disease pathology (Dotti and Salas, 2018). Thus, organoids can be useful to build a patient-specific model, enabling them to pursue the Precision Medicine approaches (Mochel et al., 2017). To accurately utilize the organoid culture technology, basic understandings of genotypic and phenotypic characteristics of organoids and similarity to the original donor are important. However, our finding suggests that the intra-heterogeneity in morphology, activity of Wnt signaling, proliferation, differentiation, and transcriptomes germane to the epithelial function of cultured organoids requires a careful interpretation of experimental results when organoid-based studies are performed.

Along the crypt-villus axis of the *in vivo* intestinal epithelium, there are morphogen gradients that regulate the proliferation and differentiation of intestinal epithelial cells. The Wnt signaling is the strongest in the basal crypt area and becomes weaker toward the villi. The strong Wnt signal in the crypt area, where intestinal stem cells are located, enables the stem cells to proliferate. Intestinal organoid culture is based on the intestinal stem cells, and the high morphogen pressure, emulating the *in vitro* stem cell niche, is necessary to maintain the culture. The ECM hydrogel structure in the organoid culture recapitulates the physical microenvironment of the *in vivo* mucosal and mesenchymal tissue structure. However, the macroscopic structure of the "dome-shaped" hydrogel does not necessarily intend to replicate the *in vivo* conditions.

In the human intestinal organoid culture, maintenance of stem cell stability and control of Wnt signaling are critical prerequisites for a long-term culture over multiple subcultures. In the conventional culture condition, the localized phosphorylated β-catenin signal was strong only on the cell-cell junction in the core organoids, whereas the signal was also dominant in the cytoplasm in the edge organoids, suggesting that the Wnt signaling in the edge organoids is more active than the core. The population of Ki67-positive cells was significantly higher in the edge organoids than those in the core, which shows a good agreement with the phosphorylated β-catenin profiles. Notably, using the same methods for passaging and culture, CRC organoids did not show this intra-heterogeneity in size difference, which can be explained by the hallmark of cancer, an abnormal proliferation (Hanahan and Weinberg, 2011), and a constitutive "turn-on" of Wnt signaling followed by the overexpression of Ki67 (Li et al., 2015; Michels et al., 2019). This observation was also concordant with the previous finding that CRC organoids do not necessarily require exogenous Wnt for growth (Sato et al., 2011), and that CRC cells acquire the ability to produce Wnt molecules (Voloshanenko et al., 2013).

We hypothesized that the concentration gradient of morphogens, here Wnt3a, inside the Matrigel dome might lead to the structural and morphological heterogeneity of organoids as a function of position in the dome. We further developed our hypothesis into three possible situations: (1) the concentration gradient of Wnt3a may be solely dependent on the diffusion of exogenous morphogens; (2) the diffused Wnt3a may be taken by the organoid cells predominantly at the edge, and less amount of Wnt3a is diffused into the core, creating a gradient; and (3) the Wnt3a may be consistently unstable under the given culture condition as a function of time. To examine the contribution of each factor in creating the spatiotemporal Wnt gradient, Wnt3a concentration was measured over time and visualized by the computer simulation. Through the simulation study by excluding the contribution of each factor at a time, we found that the instability of Wnt3a was dominant, and the physical diffusion limitation of Wnt3a in Matrigel significantly orchestrated the concentration gradient. However, the effects of cellular uptake of Wnt3a were minimal, presumably because the ECM scaffolds surrounding the organoids hinder the approach and uptake of the Wnt3a molecule to the organoids. It is noted that the pseudo-constant maintenance of the Wnt3a level by replenishing the high-Wnt medium significantly minimized the concentration gradient inside the Matrigel dome. However, as the hydrophobic nature of the Wnt molecules induces the Wnt instability (Tuysuz et al., 2017), there may be an innate limitation to avoid this unstable Wnt activity in the culture medium unless a Wnt stabilizer is applied.

The nutrient availability can be a factor that may alter the size heterogeneity of organoids in the dome-shaped hydrogel. It is noted that the chemicals, growth factors, and morphogens included in the complete medium may undergo similar diffusion limitations in the Matrigel. Thus, we do not necessarily exclude the possible effect of the nutrient gradient inside the Matrigel dome on the size heterogeneity of organoids. However, Wnt3a is not only one of the most essential morphogens in the organoid culture but also shows the inherent instability with a strong agreement with previous studies (Mihara et al., 2016; Tuysuz et al., 2017). However, there has been no critical instability issue of nutrient components, particularly glucose and amino acids in the basal medium (i.e., Advanced DMEM/F12), used in organoid cultures. Thus, it is necessary and sufficient to specifically focus on the effect of Wnt3a gradient in the current study. In addition, the weight of the Matrigel above the core organoid may not be a factor that compromises the organoid growth. First, the 3D hydrogel scaffold is the structure of numerous fibers, where liquid (here, culture medium) fills the space in the scaffolds. This network structure is not a continuous material such as liquid or solid that affects the continual mass pressure onto the organoids that are growing at each position (Asghar et al., 2013; Gelain et al., 2006). Furthermore, if the weight of hydrogel was a factor that affects the growth, the shape of organoids might have been flattened as a doughnut in the dome center. However, this flattened organoid morphology has neither been reported in any organoid-based studies nor observed in any line of intestinal organoids that we routinely grow in the laboratory. Thus, we excluded the possibility that weight of hydrogel in the current setup may hamper the organoid growth.

In the computer simulation, we provided the adjusted magnitude of color scales in each time point to accurately demonstrate the spatial Wnt3a gradient in our computational simulation setups that emulate the Wnt3a gradient generated in the conventional culture setup. The Wnt3a concentration dramatically decreases within the defined time frame, and the unified color scales used at 0 h will not accurately visualize the Wnt3a gradient at the time point that we want to specifically compare between the control and Wnt-replenished groups.

We found that multiple genes related to the epithelial physiology were significantly upregulated in the Wnt-replenished condition than the control. Especially, the upregulated genes with statistical significance in the core organoids were related to epithelial barrier function, structural change, cell growth, and differentiation, indicating that the necessary epithelial physiological functions might be compromised in the core organoids cultured under the conventional culture condition. For instance, maintaining the epithelial barrier function is a prerequisite for the homeostasis in the gut, thus the barrier dysfunction may cause the elevated chance of gut inflammation under complex luminal and vascular stimulations (Shin and Kim, 2018). The upregulated genes that we identified from the Wnt-replenished condition in the core hydrogel dome perform critical epithelial functions such as encoding the adherens junctional protein E-cadherin (*CDH1*) (Gall and Frampton, 2013) and occludin junctional protein (*OCLN*) (Furuse et al., 1993), controlling the barrier integrity in colonocytes (*VAV2*) (Rodriguez-Fdez and Bustelo, 2019), and managing the barrier function (*KLF4*) (Dang et al., 2000), where all contribute to keeping an intact

intestinal barrier. The genes related to the regulation of structural modulation are also found to be substantially upregulated in the Wnt-sufficient condition in the core dome including a transcription factor inducing epithelial-mesenchyme transition (EMT) (*SNAI1*) (Paznekas et al., 1999) and a key regulator of actin filament assembly and disassembly (*GSN*) (Sun et al., 1999). Also, the genes that are pertinent to cell growth and differentiation also showed significantly increased expression in the core dome under the high-Wnt microenvironment. For instance, we identified the genes encoding a member of EGF receptors (*ERBB2*) (Rusnak et al., 2001), regulating EMT and stem cells (*SOX9*) (Jo et al., 2014), controlling the calcium-binding function (*CALB2*) (Blum and Schwaller, 2013), managing mitochondrial translation elongation factor G1 (*GFM1*) (Hammarsund et al., 2001), encoding Notch ligands (*DLL4*) associated with the development and proliferation (*NOTCH1*) (Shutter et al., 2000), orchestrating the growth of intestinal epithelium and lineage differentiation (*HNF1A*) (D'Angelo et al., 2010), and encoding translational elongation factor (*EEF1B2*) (Pizzuti et al., 1993). Two overexpressed genes that were identified in the edge organoids under the Wnt-replenished condition are associated with the regulation of proliferation (*EPRS*) (Katsyv et al., 2016) and the morphological development (*SHROOM3*) (Grosse et al., 2011), supporting the phenotypic feature of the overgrowth of the edge organoids. As stated, this spatiotemporal gradient and instability of Wnt3a induced heterogeneous expression of MUC2 protein as a function of location. We found that the total MUC2 expression in a well was higher in the Wnt-replenished as well as in the "Adjusted" condition than the control, suggesting that the overall epithelial differentiation and major physiological function can be considerably compromised in the conventional cultures. This finding strongly supports that the hypothesis we raised is a critical factor in altering the overall cellular functions, not only in our study but also possibly in other conventional organoid cultures.

The pseudo-constant maintenance of the Wnt3a concentration in the culture medium substantially improved the Wnt instability problem in the conventional organoid medium because the level of Wnt3a in the culture medium was controlled higher than 200 ng/mL across the culture period. In addition, the high level of Wnt3a in the culture medium also provided the rapid diffusion of Wnt3a into the Matrigel core compared with the control, suggesting that both Wnt instability and diffusion limitation were mitigated under the repeated replenishment of Wnt3a. Alternatively, a Wnt stabilizer (Mihara et al., 2016; Tuysuz et al., 2017) that improves the Wnt instability may be considered to maintain the level of Wnt3a in the medium over cultures. Also, reduction of the diffusion limitation by decreasing the diffusion path (e.g., creating a smaller hydrogel dome) and enhancement of the diffusion coefficient of Wnt3a through the hydrogel (e.g., testing different hydrogels or reduced Matrigel concentration) may be compelling approaches to surmount the conventional culture challenges. Indeed, there has been a report that suggests making multiple Matrigel drops (Stewart et al., 2020), where our study explains why this approach is important. A microphysiological system may be also contemplated to maintain the steady-state Wnt concentration to the organoids introduced in the microdevice, which may, in part, resolve the diffusion limitation issue (Jin et al., 2014; Lee et al., 2018).

In conclusion, we found that Wnt3a instability and diffusion limitation in Matrigel can cause a spatiotemporal gradient of Wnt3a in a Matrigel dome where organoids are embedded in. By a careful examination of the effects of the spatiotemporal Wnt3a gradient, we discovered that intra-heterogeneity in growth and differentiation is made, which can considerably prevent accurate interpretations of a study result. This finding is significant upon a burgeoning interest of the use of organoids that has disseminated its utility to the basic science, disease modeling, tissue engineering, patient-specific validation of new drug candidates, comparative medicine using the "*in vitro* cohort" by matching to the patient cohort, evaluation of demographic effect on disease development, and Precision Medicine. We envision that our finding is potentially implementable to the cultures with other types of organoids derived from different organs, where the culture condition and data interpretation should be carefully analyzed by minimizing the unnecessary heterogeneity in each experiment.

Limitations of the Study

We only tested colonic organoids derived from either normal donors or a patient with CRC in this study. Thus, experimental results may be different when the type of organoids derived from various organs varies with divergent culture conditions. Also, the observed heterogeneity in organoid cultures may vary depending on the used hydrogel scaffold that has different physicochemical properties. The concentration gradient of Wnt3a inside a Matrigel dome was estimated by computational simulation, which may show variations from the actual local concentration of Wnt3a.

Resource Availability

Lead Contact

Further information and requests for resources and reagents should be directed to and will be fulfilled by the Lead Contact, Hyun Jung Kim (hyunjung.kim@utexas.edu).

Materials Availability

Organoid lines generated in this study are available from the Lead contact with a completed Materials Transfer Agreement.

Data and Code Availability

The published article includes all datasets generated or analyzed during this study.

METHODS

All methods can be found in the accompanying Transparent Methods supplemental file.

SUPPLEMENTAL INFORMATION

Supplemental Information can be found online at https://doi.org/10.1016/j.isci.2020.101372.

ACKNOWLEDGMENTS

We thank Dr. Jennifer McKinney for assistance in obtaining patient samples at Dell Medical School. This work was supported in part by the Bio & Medical Technology Development Program of the National Research Foundation funded by the Ministry of Science and ICT (2018M3A9H3025030 to H.J.K.), Technology Impact Award of the Cancer Research Institute (UTA18-000889 to H.J.K.), Alternatives Research and Development Foundation (UTA18-001198 to H.J.K.), the Leona M. and Harry B. Helmsley Charitable Trust (Grant #1912-03604 to H.J.K.), the National Cancer Institute of the National Institutes of Health (R21CA236690 to H.J.K.), F99/K00 Predoctoral to Postdoctoral Transition Award (1F99CA245801 to W.S.), Asan Foundation Biomedical Science Scholarship (W.S.), and Cancer Prevention and Research Institute of Texas (CPRIT) Scholar Award (#RR160093 to S.G.E.).

AUTHOR CONTRIBUTIONS

W.S. and H.J.K. designed the study and wrote the paper. W.S., A.W., S.M., Y.C.S., and H.J.K. performed experiments and analyzed data. S.G.E. and R.Y.D.F. provided clinical samples as well as scientific advice.

DECLARATION OF INTERESTS

H.J.K. is a founder of 3D Health Solutions Inc. and holds an equity interest in the company.

Received: April 2, 2020
Revised: May 22, 2020
Accepted: July 14, 2020
Published: August 21, 2020

REFERENCES

Aberle, M.R., Burkhart, R.A., Tiriac, H., Olde Damink, S.W.M., Dejong, C.H.C., Tuveson, D.A., and van Dam, R.M. (2018). Patient-derived organoid models help define personalized management of gastrointestinal cancer. Br. J. Surg. *105*, e48–e60.

Asghar, W., Shafiee, H., Chen, P., Tasoglu, S., Guven, S., Gurkan, U.A., and Demirci, U. (2013). In vitro three-dimensional cancer culture models. In Cancer Targeted Drug Delivery, Y.H. Bae, R.J. Mrsny, and K. Park, eds. (Springer), pp. 635–665.

Blum, W., and Schwaller, B. (2013). Calretinin is essential for mesothelioma cell growth/survival in vitro: a potential new target for malignant mesothelioma therapy? Int. J. Cancer *133*, 2077–2088.

Clevers, H. (2016). Modeling development and disease with organoids. Cell *165*, 1586–1597.

Crespo, M., Vilar, E., Tsai, S.Y., Chang, K., Amin, S., Srinivasan, T., Zhang, T., Pipalia, N.H., Chen, H.J., Witherspoon, M., et al. (2017). Colonic organoids derived from human induced pluripotent stem cells for modeling colorectal cancer and drug testing. Nat. Med. *23*, 878–884.

D'Angelo, A., Bluteau, O., Garcia-Gonzalez, M.A., Gresh, L., Doyen, A., Garbay, S., Robine, S., and Pontoglio, M.J.D. (2010). Hepatocyte nuclear factor 1α and β control terminal differentiation and cell fate commitment in the gut epithelium. Development *137*, 1573–1582.

Dang, D.T., Pevsner, J., and Yang, V.W. (2000). The biology of the mammalian Kruppel-like family of transcription factors. Int. J. Biochem. Cell Biol. *32*, 1103–1121.

Dedhia, P.H., Bertaux-Skeirik, N., Zavros, Y., and Spence, J.R. (2016). Organoid models of human gastrointestinal development and disease. Gastroenterology *150*, 1098–1112.

Dotti, I., and Salas, A. (2018). Potential use of human stem cell–derived intestinal organoids to

study inflammatory Bowel diseases. Inflamm. Bowel Dis. *24*, 2501–2509.

Drost, J., Karthaus, W.R., Gao, D., Driehuis, E., Sawyers, C.L., Chen, Y., and Clevers, H. (2016). Organoid culture systems for prostate epithelial and cancer tissue. Nat. Protoc. *11*, 347–358.

Ettayebi, K., Crawford, S.E., Murakami, K., Broughman, J.R., Karandikar, U., Tenge, V.R., Neill, F.H., Blutt, S.E., Zeng, X.-L., and Qu, L. (2016). Replication of human noroviruses in stem cell–derived human enteroids. Science *353*, 1387–1393.

Fair, K.L., Colquhoun, J., and Hannan, N.R.F. (2018). Intestinal organoids for modelling intestinal development and disease. Philos. Trans. R. Soc. Lond. B Biol. Sci. *373*, 20170217.

Fatehullah, A., Tan, S.H., and Barker, N. (2016). Organoids as an in vitro model of human development and disease. Nat. Cell Biol. *18*, 246–254.

Furuse, M., Hirase, T., Itoh, M., Nagafuchi, A., Yonemura, S., Tsukita, S., and Tsukita, S. (1993). Occludin - a novel integral membrane-protein localizing at tight junctions. J. Cell Biol. *123*, 1777–1788.

Gall, T.M., and Frampton, A.E. (2013). Gene of the month: E-cadherin (CDH1). J. Clin. Pathol. *66*, 928–932.

Gelain, F., Bottai, D., Vescovi, A., and Zhang, S. (2006). Designer self-assembling peptide nanofiber scaffolds for adult mouse neural stem cell 3-dimensional cultures. PLoS ONE *1*, e119.

Grosse, A.S., Pressprich, M.F., Curley, L.B., Hamilton, K.L., Margolis, B., Hildebrand, J.D., and Gumucio, D.L. (2011). Cell dynamics in fetal intestinal epithelium: implications for intestinal growth and morphogenesis. Development *138*, 4423–4432.

Hammarsund, M., Wilson, W., Corcoran, M., Merup, M., Einhorn, S., Grander, D., and Sangfelt, O. (2001). Identification and characterization of two novel human mitochondrial elongation factor genes, hEFG2 and hEFG1, phylogenetically conserved through evolution. Hum. Genet. *109*, 542–550.

Hanahan, D., and Weinberg, R.A. (2011). Hallmarks of cancer: the next generation. Cell *144*, 646–674.

Holloway, E.M., Capeling, M.M., and Spence, J.R. (2019). Biologically inspired approaches to enhance human organoid complexity. Development *146*, dev166173.

Jin, B.J., Battula, S., Zachos, N., Kovbasnjuk, O., Fawlke-Abel, J., In, J., Donowitz, M., and Verkman, A.S. (2014). Microfluidics platform for measurement of volume changes in immobilized intestinal enteroids. Biomicrofluidics *8*, 024106.

Jo, A., Denduluri, S., Zhang, B., Wang, Z.L., Yin, L.J., Yan, Z.J., Kang, R., Shi, L.L., Mok, J., Lee, M.J., et al. (2014). The versatile functions of Sox9 in development, stem cells, and human diseases. Genes Dis. *1*, 149–161.

Kassis, T., Hernandez-Gordillo, V., Langer, R., and Griffith, L.G. (2019). OrgaQuant: human intestinal organoid localization and quantification using deep convolutional neural networks. Sci. Rep. *9*, 12479.

Katsyv, I., Wang, M.H., Song, W.M., Zhou, X.X., Zhao, Y.Z., Park, S., Zhu, J., Zhang, B., and Irie, H.Y. (2016). EPRS is a critical regulator of cell proliferation and estrogen signaling in ER+ breast cancer. Oncotarget *7*, 69592–69605.

Koch, S. (2017). Extrinsic control of Wnt signaling in the intestine. Differentiation *97*, 1–8.

Lee, K.K., McCauley, H.A., Broda, T.R., Kofron, M.J., Wells, J.M., and Hong, C.I. (2018). Human stomach-on-a-chip with luminal flow and peristaltic-like motility. Lab Chip *18*, 3079–3085.

Li, L.T., Jiang, G., Chen, Q., and Zheng, J.N. (2015). Ki67 is a promising molecular target in the diagnosis of cancer. Mol. Med. Rep. *11*, 1566–1572.

Li, X., Nadauld, L., Ootani, A., Corney, D.C., Pai, R.K., Gevaert, O., Cantrell, M.A., Rack, P.G., Neal, J.T., Chan, C.W., et al. (2014). Oncogenic transformation of diverse gastrointestinal tissues in primary organoid culture. Nat. Med. *20*, 769–777.

Mah, A.T., Yan, K.S., and Kuo, C.J. (2016). Wnt pathway regulation of intestinal stem cells. J. Physiol. *594*, 4837–4847.

Michels, B.E., Mosa, M.H., Grebbin, B.M., Yepes, D., Darvishi, T., Hausmann, J., Urlaub, H., Zeuzem, S., Kvasnicka, H.M., Oellerich, T., et al. (2019). Human colon organoids reveal distinct physiologic and oncogenic Wnt responses. J. Exp. Med. *216*, 704–720.

Mihara, E., Hirai, H., Yamamoto, H., Tamura-Kawakami, K., Matano, M., Kikuchi, A., Sato, T., and Takagi, J. (2016). Active and water-soluble form of lipidated Wnt protein is maintained by a serum glycoprotein afamin/alpha-albumin. eLife *5*, e11621.

Mochel, J.P., Jergens, A.E., Kingsbury, D., Kim, H.J., Martin, M.G., and Allenspach, K. (2017). Intestinal stem cells to advance drug development, precision, and regenerative medicine: a paradigm shift in translational research. AAPS J. *20*, 17.

Nakamura, T., and Sato, T. (2018). Advancing intestinal organoid technology toward regenerative medicine. Cell Mol. Gastroenterol. Hepatol. *5*, 51–60.

Nanki, K., Fujii, M., Shimokawa, M., Matano, M., Nishikori, S., Date, S., Takano, A., Toshimitsu, K., Ohta, Y., Takahashi, S., et al. (2020). Somatic inflammatory gene mutations in human ulcerative colitis epithelium. Nature *577*, 254–259.

Ohta, Y., and Sato, T. (2014). Intestinal tumor in a dish. Front. Med. *1*, 14.

Paznekas, W.A., Okajima, K., Schertzer, M., Wood, S., and Jabs, E.W. (1999). Genomic organization, expression, and chromosome location of the human SNAIL gene (SNAI1) and a related processed pseudogene (SNAI1P). Genomics *62*, 42–49.

Pizzuti, A., Gennarelli, M., Novelli, G., Colosimo, A., Lo Cicero, S., Caskey, C.T., and Dallapiccola, B. (1993). Human elongation factor EF-1 beta: cloning and characterization of the EF1 beta 5a gene and assignment of EF-1 beta isoforms to chromosomes 2,5,15 and X. Biochem. Biophys. Res. Commun. *197*, 154–162.

Rodriguez-Fdez, S., and Bustelo, X.R. (2019). The Vav GEF family: an evolutionary and functional perspective. Cells *8*, 465.

Rusnak, D.W., Affleck, K., Cockerill, S.G., Stubberfield, C., Harris, R., Page, M., Smith, K.J., Guntrip, S.B., Carter, M.C., Shaw, R.J., et al. (2001). The characterization of novel, dual ErbB-2/EGFR, tyrosine kinase inhibitors: potential therapy for cancer. Cancer Res. *61*, 7196–7203.

Sato, T., and Clevers, H. (2013). Growing self-organizing mini-guts from a single intestinal stem cell: mechanism and applications. Science *340*, 1190–1194.

Sato, T., Stange, D.E., Ferrante, M., Vries, R.G., Van Es, J.H., Van den Brink, S., Van Houdt, W.J., Pronk, A., Van Gorp, J., Siersema, P.D., et al. (2011). Long-term expansion of epithelial organoids from human colon, adenoma, adenocarcinoma, and Barrett's epithelium. Gastroenterology *141*, 1762–1772.

Schwank, G., Koo, B.K., Sasselli, V., Dekkers, J.F., Heo, I., Demircan, T., Sasaki, N., Boymans, S., Cuppen, E., van der Ent, C.K., et al. (2013). Functional repair of CFTR by CRISPR/Cas9 in intestinal stem cell organoids of cystic fibrosis patients. Cell Stem Cell *13*, 653–658.

Shin, W., and Kim, H.J. (2018). Intestinal barrier dysfunction orchestrates the onset of inflammatory host-microbiome cross-talk in a human gut inflammation-on-a-chip. Proc. Natl. Acad. Sci. U S A *115*, E10539–E10547.

Shutter, J.R., Scully, S., Fan, W., Richards, W.G., Kitajewski, J., Deblandre, G.A., Kintner, C.R., and Stark, K.L. (2000). Dll4, a novel Notch ligand expressed in arterial endothelium. Gene Dev. *14*, 1313–1318.

Stewart, C.J., Estes, M.K., and Ramani, S. (2020). Establishing human intestinal enteroid/organoid lines from preterm infant and adult tissue. In Innate Lymphoid Cells, S. Amarnath, ed. (Springer), pp. 185–198.

Sugimoto, S., and Sato, T. (2017). Establishment of 3D intestinal organoid cultures from intestinal stem cells. Methods Mol. Biol. *1612*, 97–105.

Sun, H.Q., Yamamoto, M., Mejillano, M., and Yin, H.L. (1999). Gelsolin, a multifunctional actin regulatory protein. J. Biol. Chem. *274*, 33179–33182.

Tuysuz, N., van Bloois, L., van den Brink, S., Begthel, H., Verstegen, M.M., Cruz, L.J., Hui, L., van der Laan, L.J., de Jonge, J., Vries, R., et al. (2017). Lipid-mediated Wnt protein stabilization enables serum-free culture of human organ stem cells. Nat. Commun. *8*, 14578.

Urbischek, M., Rannikmae, H., Foets, T., Ravn, K., Hyvonen, M., and de la Roche, M. (2019). Organoid culture media formulated with growth factors of defined cellular activity. Sci. Rep. *9*, 6193.

Voloshanenko, O., Erdmann, G., Dubash, T.D., Augustin, I., Metzig, M., Moffa, G., Hundsrucker, C., Kerr, G., Sandmann, T., Anchang, B., et al. (2013). Wnt secretion is required to maintain high levels of Wnt activity in colon cancer cells. Nat. Commun. *4*, 2610.

Yui, S., Nakamura, T., Sato, T., Nemoto, Y., Mizutani, T., Zheng, X., Ichinose, S., Nagaishi, T., Okamoto, R., and Tsuchiya, K. (2012). Functional engraftment of colon epithelium expanded in vitro from a single adult Lgr5+ stem cell. Nat. Med. *18*, 618–623.

iScience, Volume *21*

Supplemental Information

Spatiotemporal Gradient and Instability of Wnt Induce Heterogeneous Growth and Differentiation of Human Intestinal Organoids

Woojung Shin, Alexander Wu, Soyoun Min, Yong Cheol Shin, R. Y. Declan Fleming, S. Gail Eckhardt, and Hyun Jung Kim

Table S1. Constants and equations used in the COMSOL computer simulation. Related to Figure 3.

Parameter	Description	Quantity	References
C_0	Initial concentration of Wnt	1×10^{-5} mol/m^3	Figure 2A, 2B[a]
D_{medium}	Diffusion coefficient of Wnt in medium	6.90×10^{-9} m^2/s	Sick et al., 2006; Shin et al., 2019
$D_{matrigel}$	Diffusion coefficient of Wnt in Matrigel	2.78×10^{-10} m^2/s	Kihara et al., 2013
R_{rep}	Rate of Wnt decay in Wnt_{rep}	-5.32×10^{-12} mol/m^{3}s	Figure 3A[a]
$R_{control}$	Rate of Wnt decay in Control	$-C_0\times3\times10^{-5}e^{-3\times10^{-5}t}$ mol/m^{3}s	Figure 2B[a]
R_{uptake}	Wnt uptake by organoids	$-4\times10^{-10}e^{-6.05\times10^{-5}t}$ mol/m^{3}s	Figure 2B[a]

[a]The quantity of each parameter was experimentally determined from the indicated figures.

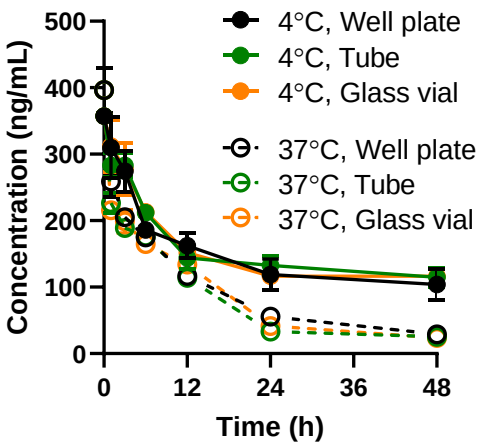

Figure S1. Concentration profile of the Wnt3a in the complete medium incubated in different containers. Related to Figure 2. Wnt3a concentration in the complete medium was decreased over time regardless of the container type. Complete medium was incubated in a well of 24 well plate (“Well plate”, black), 1.5 mL microcentrifuge tube (“Tube”, green), or 2 mL glass vial (“Glass vial”, orange) at either 4°C or 37°C for 48 h. Wnt3a concentration in the collected medium at each time point was measured using the cell-based luciferase assay. N=3.

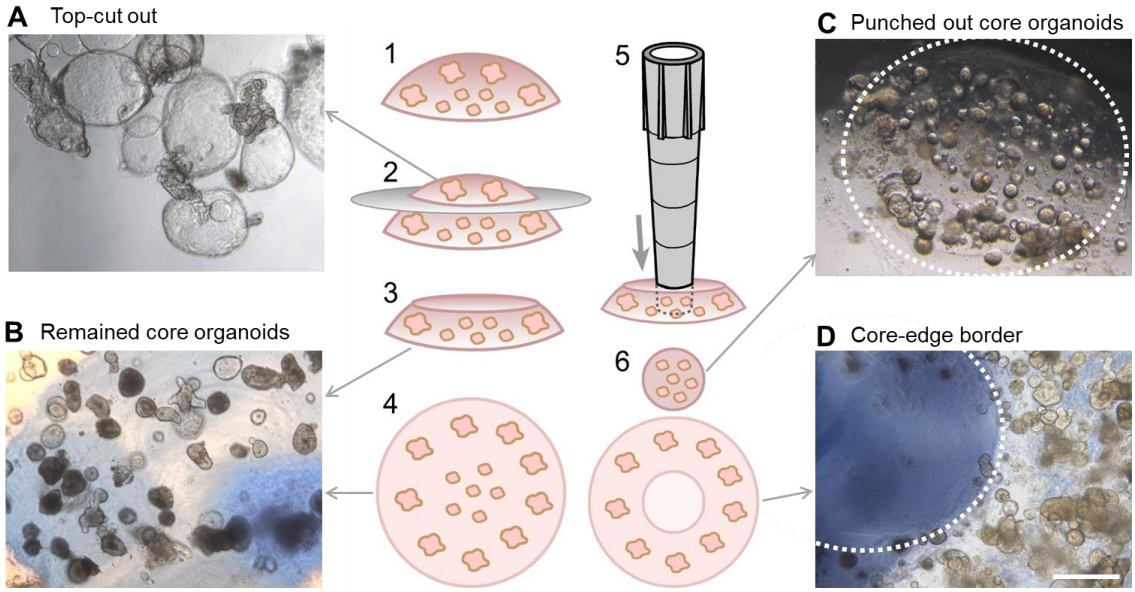

Figure S2. A procedure to harvest the organoids located in the core or edge. Related to Figure 2 and Figure 4. (A) To harvest the core or the edge organoids independently from a Matrigel dome (Step 1), a cell scraper (5 mm width; ABI Scientific Inc.) was used to cut out the top part of a dome (Step 2). (B) After the removal of the top-cut part (Steps 3 and 4), the remained core organoids were used for the isolation process. (C) A cut P200 micropipette (outer diameter, 3 mm) was located in the middle of the top-cut Matrigel to collect the core organoids by gently sucking the part up. The collected core organoids were transferred to a sterilized microcentrifuge tube (1.5 mL; Steps 5 and 6). (D) Once the core organoids are removed, the edge organoids were then collected using a new sterile pipet tip. Bar, 500 µm.

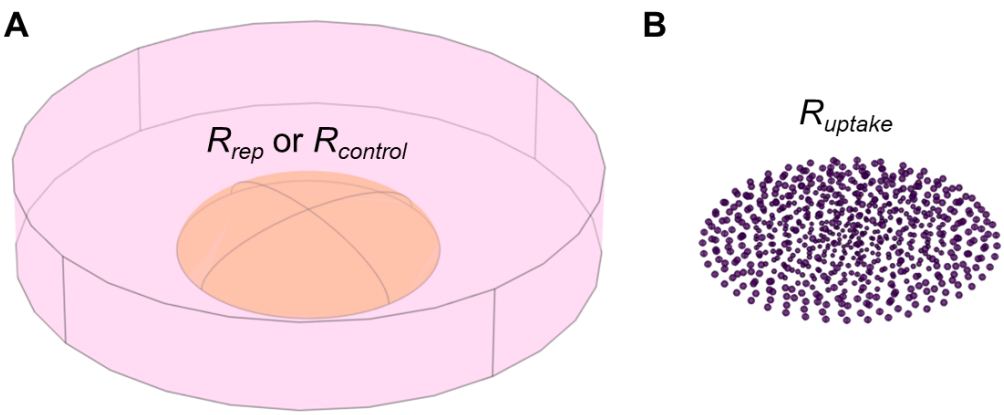

Figure S3. Domains that are applied with reaction terms in the COMSOL simulation. Related to Figure 3. To calculate the concentration profile of Wnt3a in the computational simulation, each geometrical domain was set with different reaction rates. (A) The rates of Wnt decay in the Wnt3a replenished condition (R_{rep}) or conventional culture setup ($R_{control}$) were applied in both Matrigel and medium domains. (B) The rate of Wnt3a uptake by organoids (R_{uptake}) was set in the organoid domain.

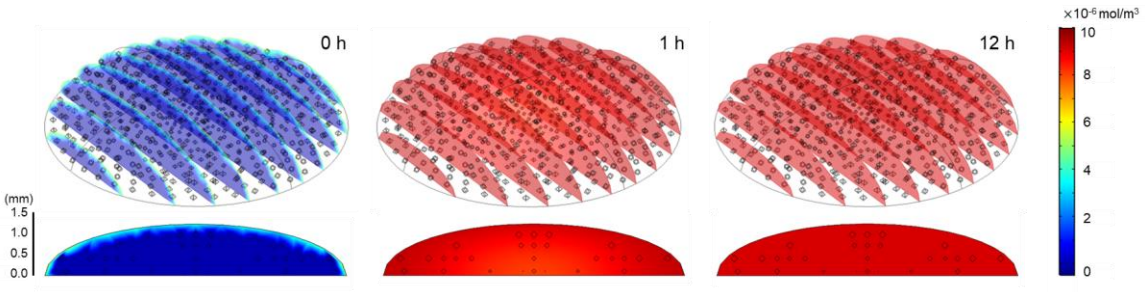

Figure S4. Spatiotemporal gradient of Wnt3a in the Wnt-replenished condition with the fixed color scale. Related to Figure 3. The profile of Wnt3a concentration in the Matrigel dome, shown in Figure 3D, was represented with the fixed color scale. In this concentration range, no significant spatial gradient of Wnt3a was observed, whereas the modular scale successfully demonstrated the intra-heterogeneity of Wnt3a concentration inside the Matrigel dome.

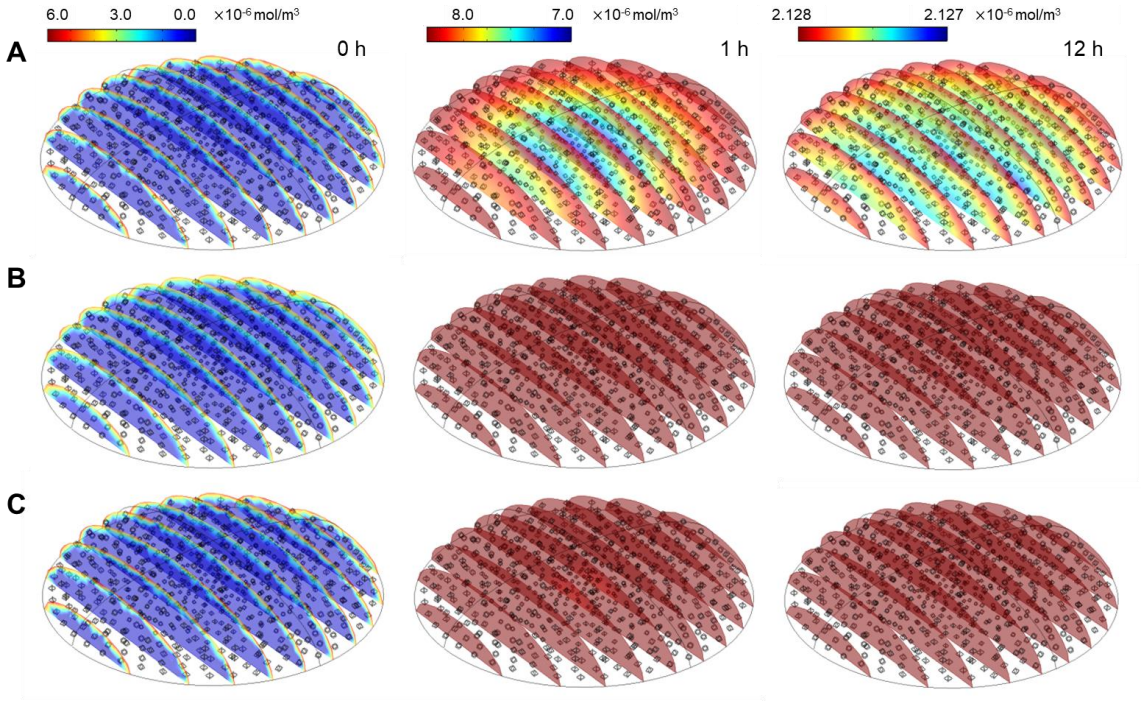

Figure S5. A computational investigation to identify the contributing factor in generating the Wnt3a gradient inside the Matrigel dome. Related to Figure 3. We performed the COMSOL computational simulation to identify the effect of cellular uptake (A), diffusion limitation inside the dome (B), and the instability of Wnt3a in the culture medium (C) on the generation of Wnt3a gradient. The individual factor defined in A to C was independently removed, respectively, from the boundary condition of the simulation, then the simulation was performed to identify the contributing factor that creates the spatiotemporal Wnt3a gradient.

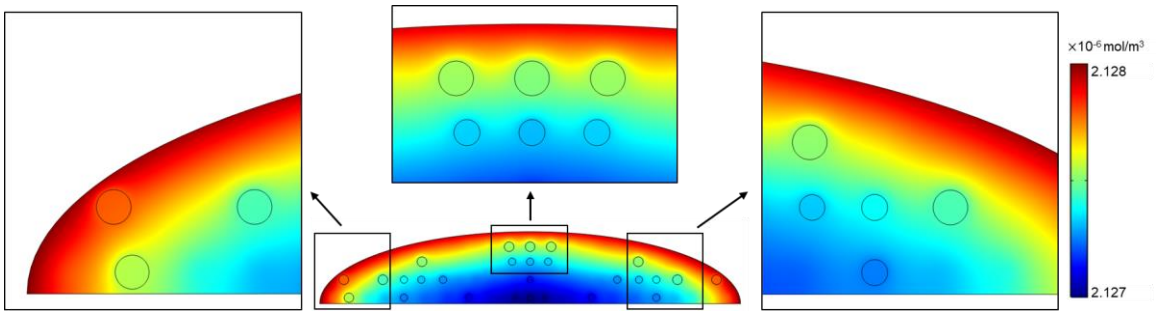

Figure S6. Local gradient of Wnt3a generated by the cellular Wnt3a uptake. Related to Figure 3. Subtle local gradient was generated around the organoids embedded in Matrigel, visualized by the COMSOL computer simulation. The condition of the conventional culture at 12 h was used for the visualization. The circular shapes in the captured figures represent intestinal organoids in the Matrigel dome. The captured figure is a cross-sectional view of the center of the Matrigel dome in XZ direction.

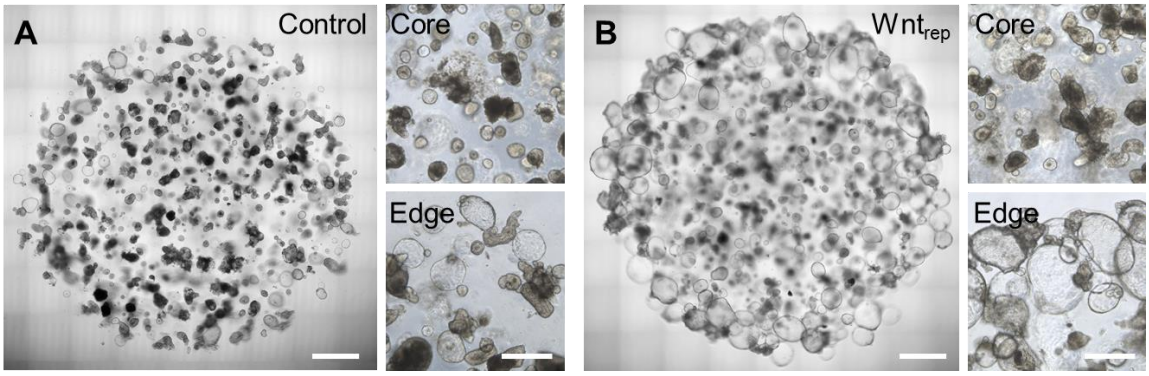

Figure S7. A morphological assessment of the size distribution of organoids in response to the repeated replenishment of a culture medium. Related to Figure 3 and Figure 4. (A) Stitched images (left) and high-magnification images of “Core” (top right) and “Edge” (bottom right) organoids grown for 6 days in the conventional culture medium (A; Control) and Wnt3a replenished condition (B; Wnt_{rep}). Scale bars of the stitched images and the high magnification images are 1 mm and 500 μm, respectively. Phase contrast microscopy was applied to acquire stitched or high-power micrographs on day 6.

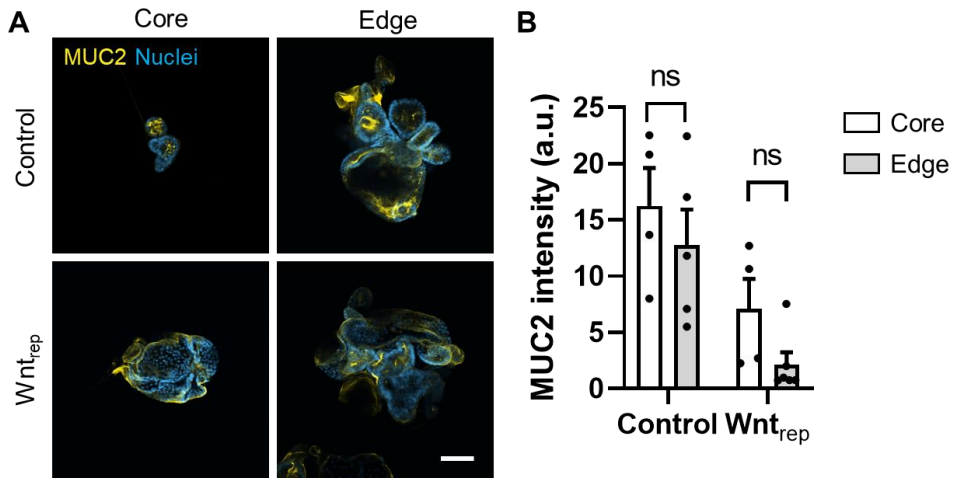

Figure S8. Expression of MUC2 in the organoids cultured in a complete medium without additional differentiation step. Related to Figure 4. (A) Immunofluorescence visualization of MUC2 in the organoids cultured in either conventional (Control) or Wnt-replenished condition (Wnt_{rep}) for 6 days. Differentiation was not induced in all experimental groups. Bar, 100 µm. (B) Quantification of the averaged MUC2 expression per organoids presented in "A" (Control-core, N=4, Control-edge, N=5, Wnt_{rep}-core, N=4, Wnt_{rep}-edge, N=6). Data are represented as mean ± SEM. Two-way ANOVA was performed to evaluate statistical significance of the differences. ns, not significant.

Transparent Methods

Generation of human intestinal organoids. The healthy colonic organoid line, C103, was purchased from The Gastrointestinal Experimental Model Systems Core at the Baylor College of Medicine. Thus, the original subject's information is not reported. The CRC organoid was derived from a surgical resection from a patient (Male, 60 years-old) with rectosigmoid adenocarcinoma under the approval of The University of Texas at Austin Institutional Research Board (IRB# 2017-06-0114).

To generate a colorectal cancer (CRC) organoid line from a CRC tissue, a CRC tissue resection examined by a pathological doctor was cut into ~1 cm piece from the surgical resection and brought to lab within 1 h on ice. Tissue was washed with ice-cold phosphate buffer saline (PBS; Gibco) supplemented with penicillin/streptomycin (Pen/Strep, 100 U/mL and 100 µg/mL; Thermo Fisher Scientific) three times and diced with a razor blade. Tissue fragments were digested in 10 mL of collagenase type I (2 mg/mL; Sigma) dissolved in Advanced Dulbecco's Modified Eagle Medium/F12 (Advanced DMEM/F12, Gibco) supplemented with 2% (v/v) fetal bovine serum (FBS; Gibco) and incubated at 37°C for 40 min. After the enzymatic reaction, the digested tissue was washed two times with Advanced DMEM/F12 supplemented with Pen/Strep, 1× GlutaMAX, and 10 mM HEPES by centrifugation at 300×*g* for 3 min. After the centrifugation, tissue pellet was suspended in Matrigel and 30 µL of Matrigel-tissue suspension was dropped in each well of a 24-well plate. After incubating the plate in a humidified CO_2 incubator (Eppendorf) for 10 min for gelation, 500 µL of the complete medium was added.

Culture of human intestinal organoids. For the conventional culture of organoids, both normal and CRC organoids were embedded in the Matrigel (Corning) and cultured at 37°C, 5% CO_2, humidified condition by changing the complete medium (500 µL per well) every other day for up to 7 days. The base medium was prepared by adding murine recombinant epidermal growth factor (EGF, 50 ng/mL; Peprotech), SB202190 (30 µM; Sigma), A-8301 (500 nM; Sigma), gastrin (10 nM; Sigma), *N*-acetylcysteine (1 mM; MP Biomedicals), nicotinamide (10 mM; Sigma), N2 (1×; R&D Systems), B27 (1×; Gibco), human recombinant Wnt (100 ng/mL; Novus Biologicals), Primocin (100 µg/mL; Invivogen), and Y-27632 (10 µM; STEMCELL Technologies) in Advanced DMEM/F12 (Gibco). Next, three conditioned media of Wnt3a, R-spondin, and Noggin were mixed with the base medium with the volume ratio of 75:10:5:10% (v/v). The conditioned medium of Wnt3a, R-spondin, and Noggin was independently prepared by culturing L-WNT-3A (ATCC, CRL2647), Rspo1 (Trevigen) and Noggin HEK293 (Baylor College of Medicine). For Wnt3a conditioned medium, L-WNT-3A cells that had been cultured in DMEM supplemented with 10% FBS and Geneticin (400 µg/mL; Gibco) were cultured in 10 mL of Advanced DMEM/F12 supplemented with 1× GlutaMAX and 8% FBS per one T-75 flask for 1 week. Supernatant was collected after 4 days and kept at 4°C (1st collection). The same amount of fresh medium was added to the flask, and supernatant was collected after another 3 days (2nd collection). Harvested 1st

and 2nd media were filtered through 0.22 μm pores and mixed with the equal volume ratio. Prepared conditioned medium was aliquoted and kept at -80°C until use. To harvest R-spondin conditioned medium, Rspo1 cells cultured in DMEM supplemented with 10% FBS and Zeocin (300 μg/mL; Thermo Fisher Scientific) were cultured in 20 mL of Advanced DMEM/F12 supplemented with 1× GlutaMAX and 8% (v/v) FBS per one T-75 flask for 1 week. Supernatant was collected, filtered through 0.22 μm pores, and kept at -80°C until use. For preparing Noggin conditioned medium, Noggin HEK293 cells cultured in DMEM supplemented with 10% FBS and puromycin (10 μg/mL; Sigma) were cultured in 20 mL of Advanced DMEM/F12 supplemented with 1× GlutaMAX and 8% FBS per one T-75 flask for 1 week. Supernatant was collected, filtered through 0.22 μm pores (CELLTREAT Scientific), and kept at -80°C until use.

For the Wnt-replenished cultures, the complete medium was replenished every 3 h by changing the cultured medium to the fresh complete medium that was kept frozen at -80°C to minimize the temperature-dependent decrease of Wnt3a concentration.

Once organoids are grown for 6-8 days, the organoids are passaged by adding 500 μL of the Cell Recovery Solution (Corning) in each well that contains organoid-embedded Matrigel, followed by the incubation at 4°C for 30 min for dissolving the Matrigel (Corning). Organoids collected from a plate (~12 mL) were then transferred in a sterile 15 mL conical tube (Corning), pelleted by centrifugation at 100×*g* for 5 min, mixed with 1 mL of TrypLE Express (Gibco) after aspiration, then incubated at 37°C for 2 min for the dissociation. After the enzymatic fragmentation, 4 mL of 10% (v/v) fetal bovine serum (FBS)-containing phosphate buffered saline (PBS) was added, then the solution was mixed by pipetting with a P1000 micropipette 20 times. After spin down (100×*g* for 5 min) and aspiration, Matrigel was added to the organoid fragments, well-dispersed by pipetting more than 20 times for ~30 s, then an aliquot (30 μL) of Matrigel-fragment suspension was dropped to the well in a 24-well plate. Once the gelation is over at 37°C for 15 min, 500 μL of complete medium was added for the organoid culture. The size distribution of initial organoid fragments was uniform regardless of the location inside the dome-shaped Matrigel.

To induce organoid differentiation in transcriptome analysis and MUC2 expression analysis, the differentiation medium was made based on a protocol that leads to the enhanced goblet cell population (Sato et al., 2011). The differentiation medium is depleted with Wnt3a, R-Spondin, SB202190, and nicotinamide with a ½ reduced amount of Noggin from the complete medium. The reduced volume due to the removal of the Wnt3a and R-Spondin conditioned medium was filled with Advanced DMEM/F12 (Gibco) supplemented with Pen/Strep, 1× GlutaMAX (Gibco), and 10 mM HEPES (Gibco). Organoids cultured for 3 days in the complete medium was applied with the differentiation medium for another 3 days to induce differentiation. When MUC2 expression was analyzed without differentiation, the complete medium was used with either the conventional culture or Wnt-replenished condition.

Culture of Wnt reporter cells. The Wnt reporter cells (an engineered 3T3 mouse fibroblast cell line) were cultured in the growth medium (DMEM, Gibco;

10% (v/v) fetal bovine serum; and Pen/Strep, 100 U/mL and 100 µg/mL) in a 100 mm tissue culture dish. Cells at passage number 3-5 was used for the assay. To perform the quantification assay, the cultured cells were trypsinized (0.05% Trypsin/EDTA, Gibco) at 37°C for 3 min, collected in a sterilized 15 mL conical tube (Corning), pelleted by a centrifugation at 300×*g* at 37°C for 3 min. Cells were suspended in DMEM supplemented with 25 mM HEPES, and 50 µL of cell suspension was added per well in an opaque 96 well plate with 6×10^5 cells/mL density. The plate was incubated in a humidified CO_2 incubator for overnight.
Wnt stability test. Cell-based luciferase assay was used to quantify Wnt3a concentration based on a manufacturer's protocol (LEADING LIGHT Wnt Reporter Assay; Enzo Life Sciences). Once the Wnt reporter cells were prepared in the 96-well cell culture plate, an aliquot of the sample (100 µL) was added to each well, incubated in a 5% CO2 incubator at 37°C for 20 h, then the luciferase assay solution (100 µL; Promega) was added to each well after aspiration of the reaction medium. After 10 min of incubation under light protection, the luminescence of the luciferase signal was detected using a microplate reader (SpectraMax i3; Molecular Devices). The concentration of Wnt3a was estimated based on the standard curve. To analyze the stability of the Wnt3a in the complete medium depending on the incubation time and container material, we aliquoted 500 µL of the complete medium into individual containers, a microcentrifuge tube (1.5 mL; Axygen), a glass vial (2 mL; Thomas Scientific), or a well plate (24-well; Corning). After we incubated these setups at either 4°C or 37°C for 48 h, we measured the level of Wnt3a concentration as described.
Image Analysis. The morphology of organoids was observed and recorded using phase-contrast (DMi1; Leica), differential interference contrast (DIC), and a laser-scanning fluorescence confocal microscopy (DMi8; Leica). Acquired images were analyzed using LAS X (Leica) or ImageJ. Stitching analysis was performed with either a DMi8 microscope system (Leica) using a stitching function on the LASX software (Leica) or DMi1 inverted phase contrast microscope by taking images in a sequence and manually stitching the images.

To assess the abundance of the aged organoids, the number of organoids in a well was first counted and organoids with pixel intensity higher than 100 was counted as the aged organoids to calculated the ratio. The analysis was performed on ImageJ.

To perform immunofluorescence visualization, organoids cultured in Matrigel was treated with 500 µL of paraformaldehyde (PFA, 4% w/v; Electron Microscopy Sciences) and incubated at room temperature for 30 min. PFA degrades Matrigel and fixes organoids at the same time. Fixed organoids were collected in a 1.5 mL microcentrifuge tube and pelleted by spinning for 5 s in a bench-top centrifuge. Supernatant was removed and organoids were washed with 500 µL of deionized water (DW) by centrifugation. Organoids were then suspended in 100 µL of DW, added to a glass bottom dish (Matsunami), then the dish was incubated at room temperature for 1 h to let organoids adhere to the glass surface. Once organoids are attached, DW was removed and organoids were permeabilized with Triton X-100 (0.3% v/v, Sigma) for 30 min, washed with PBS (Ca^{2+}- and Mg^{2+}-free; Gibco) two times, then blocked with bovine serum

albumin (BSA, 2% w/v, Hyclone Laboratories, Inc.) for 1 h, all performed at room temperature. Primary antibodies diluted with 2% (w/v) BSA solution was added and incubated for 1 h at room temperature or overnight at 4°C. Organoids were then washed twice with PBS and secondary antibodies (anti-rabbit IgG H&L labeled with DyLight 488 or anti-mouse IgG H&L conjugated with DyLight 488; Abcam) diluted with 2% (w/v) BSA solution was added and incubated for 1 h at room temperature. After washing with PBS, nuclei and F-actin staining was performed using 4',6-diamidino-2-phenylindole dihydrochloride (DAPI; 5 μg/mL; Thermo Scientific) or Alexa Fluor 647 Phalloidin (330 nM; Thermo Fisher Scientific), respectively, at room temperature for 30 min. Stained organoids were washed twice with PBS, submerged with a Prolong Gold Antifade reagent with DAPI (Thermo Fisher Scientific), and covered with a cover glass (Corning). To visualize phosphorylated β-catenin, Ki67, and MUC2, monoclonal anti-β-catenin (Cell Signaling Technology), polyclonal anti-Ki67 (Abcam), and monoclonal anti-MUC2 (Santa Cruz Biotechnology) antibodies were used. Concentration of each antibody was followed by the manufacturer's instruction.

Fluorescence imaging was performed using the DMi8 microscope (Leica) equipped with the TCS SPE confocal system with solid state excitation laser sources of 405 nm, 488 nm, 532 nm, and 635 nm and an Ultra high dynamic PMT detector. Images were obtained using a 10× objective (NA 0.3; dry immersion; Leica) and image analysis was performed on the LASX software (Leica). When the population of Ki67-positive cells was quantified, z-stacked images were obtained and 3D reconstruction images were obtained using a module installed on the LASX software. ImageJ software (ver. 1.52i) was used to count the total number of cells, counted by the number of nuclei, as well as the number of Ki67-positive cells. To quantify MUC2 intensity, ImageJ software was used and integrative intensity per organoid was measured.

Computational simulation. A finite element method was used in COMSOL Multiphysics 5.3 (COMSOL Inc.) to predict the Wnt3a concentration inside the Matrigel dome. Transport of diluted species with the time-dependent study was used. To compute molecular transport, Fick's second law with reaction terms was applied, following the equations below,

$$\frac{\partial C}{\partial t} + \nabla \cdot J = R$$
$$J = -D\nabla C$$

where C, concentration (mol/m^3), t, time (s), J, flux (mol/m^{2}s), R, reaction rate (mol/m^{3}s), D, diffusion coefficient (m^2/s).

The geometry of the Matrigel and medium domains were drawn based on the actual dimensions, where the Matrigel dome, having 7 mm diameter and 1.2 mm height, was placed on a well of 24-well plate, filled with 500 μL medium. The number and size of organoids drawn in the geometry were also based on the actual measurements. For the visualization of the study results, we showed only the Matrigel area to highlight the concentration profile existing in the gel. Therefore, there is no discontinuity between the medium area and the Matrigel dome. The medium area in the simulation was set as a single material with the fixed diffusion coefficient. Therefore, Wnt3a in the medium was assumed to be

well mixed, which reflects the experimental condition. At time 0, concentration in the medium domain was set to the initial concentration, C_0, and concentrations in the Matrigel- and organoid domains were set to 0. In the simulation, we set the minimum concentration of Wnt3a as 0, so that concentration would not drop to negative values.

To reflect the decomposition of Wnt3a in the culture medium, an exponential regression equation and a linear regression equation obtained from the "Control" in Figure 2B and "Wnt_{rep}" in Figure 3A, respectively, was used to calculate reaction terms in each condition. In case of the "Control" condition, an exponentially decreasing equation was obtained as follows,

$$C_t = C_0 \times e^{-3\times10^{-5}t}$$

where C_t indicates Wnt3a concentration at time t, and C_0 indicated the initial Wnt3a concentration in the complete medium. Using this equation, we obtained the decay rate, $R_{control}$, as follows.

$$R_{control} = \frac{dC(t)}{dt} = -C_0 \times 3 \times 10^{-5} \times e^{-3\times10^{-5}t}$$

In case of the "Wnt_{rep}" condition, the obtained regression equation is as follows,

$$C_t = -5.32 \times 10^{-12} \times t + C_0$$

where the decay rate of Wnt3a, R_{rep}, was derived as follows.

$$R_{rep} = \frac{dC(t)}{dt} = -5.32 \times 10^{-12}$$

The rate of Wnt3a uptake by organoids was calculated from the difference between the "Control" and "+Organoid" groups in Figure 2B. Parameters used in the simulation are provided in Table S1. The calculated $R_{control}$ and R_{rep} were applied in the medium- and Matrigel domains in the simulations of Control and Wnt_{rep}, respectively. The cellular uptake was defined specifically in the organoid bodies drawn in the simulation, not uniformly across Matrigel or Medium domain.

For the stability and convergence conditions, we used a physics-controlled "Normal" element size setting on COMSOL Multiphysics software. We performed a "Time-dependent" study, where we calculated the concentration profile with a 30 min time gap. In terms of the accuracy of the simulation results, iterations and convergence were performed on COMSOL. Specifically, we used the generalized minimal residual (GMRES) method with the residual tolerance of 0.01. We also performed 50 times of iterations before the start. Furthermore, we used the backward differentiation formula (BDF) method for time-stepping to increase the stability of the simulation results. Mesh size was set with a predefined "Extremely fine" condition, where detailed settings are as follows. Maximum element size, 0.312 mm, minimum element size, 0.00312 mm, maximum element growth rate, 1.3, curvature factor, 0.2, and resolution of narrow regions, 1.

Transcriptomic analysis. Core and edge organoids grown for 6 days were harvested respectively using the method described in the main text (Figs. 2C and S2). Organoids collected in 1.5 mL microcentrifuge tubes were pelleted by using a bench-top mini-centrifuge (Ohaus) at room temperature for 5 s. The TRIzol reagent (1 mL; Thermo Fisher Scientific) was added to isolate total RNA from the organoid pellet once the supernatant was aspirated. To synthesize cDNA, RT^2 First Strand Kit (Qiagen) was used by following the manufacturer's protocol. To

run quantitative polymerase chain reaction (qPCR) analysis, synthesized cDNA solution was mixed with RT^2 SYBR Green ROX qPCR Mastermix (Qiagen), and 20 µL of the mixture was added to each well of GeneQuery Human Epithelial Cell Biology qPCR Array Kit (ScienCell). PCR reaction was performed using a Quantstudio 3 real-time PCR system (Applied Biosystems) following the sequence of 95°C for 10 min and 40 cycles at 95°C for 20 s, 65°C for 20 s, and 72°C for 20 s. The results were displayed using an online-based data analysis tool, Heatmapper (Babicki et al., 2016). Raw ΔCT values, averaged from three replicates, were used and *LDHA* was used as a reference gene. Average Linkage method was used for clustering, and Euclidean method was used for distance measurement.

Quantification and Statistical Analysis

A one-tailed or two-tailed unpaired t-test was performed to compare the significant differences between the two groups. One-way or two-way analysis of variance (ANOVA) with multiple comparisons was studied when multiple groups were compared. All the error bars represent ± SEM (standard error of the mean). All the statistical analysis, including regression analysis, was performed using GraphPad Prism 8.3 (GraphPad Software Inc.).